Long-Range Interactions in Salt-in-Ionic Liquids

Xuhui Zhang, Zachary A. H. Goodwin*, Alexis G. Hoane, Alex Deptula, Daniel M. Markiewitz, Nicola Molinari, Qianlu Zheng, Hua Li, Michael McEldrew, Boris Kozinsky, Martin Z. Bazant, Cecilia Leal, Rob Atkin, Andrew Gewirth, Mark W. Rutland, Rosa Espinosa-Marzal*

*corresponding authors

Xuhui Zhang

E-mail: xuhui2@illinois.edu

Department of Civil and Environmental Engineering, University of Illinois at Urbana-Champaign, Urbana, Illinois 61801, USA

Zachary A. H. Goodwin*

E-mail: zgoodwin@seas.harvard.edu

John A. Paulson School of Engineering and Applied Sciences, Harvard University, Cambridge, MA 02138, USA

Department of Materials, Imperial College of London, South Kensington Campus, London SW7 2AZ, UK

Alexis G. Hoane

E-mail: ahoane2@illinois.edu

Department of Chemistry, University of Illinois at Urbana−Champaign, Urbana, Illinois 61801, United States

Alex Deptula

E-mail: deptula2@illinois.edu

Department of Materials Science and Engineering, University of Illinois at Urbana-Champaign, Urbana, Illinois 61801, USA

Daniel M. Markiewitz

E-mail: dmm385@mit.edu

Department of Chemical Engineering, Massachusetts Institute of Technology, Cambridge, MA, USA

Nicola Molinari

E-mail: nmolinari@seas.harvard.edu

John A. Paulson School of Engineering and Applied Sciences, Harvard University, Cambridge, MA 02138, USA

Robert Bosch LLC, Research and Technology Center, Cambridge, MA 02142, USA

Qianlu Zheng

E-mail: qianluz2@illinois.edu

Department of Civil and Environmental Engineering, University of Illinois at Urbana-Champaign, Urbana, Illinois 61801, USA

Hua Li:

E-mail: Hua.Li@uwa.edu.au

[1]School of Molecular Sciences, The University of Western Australia, Perth, Western Australia, Australia, 6009

[2]Centre for Microscopy, Characterisation and Analysis, The University of Western Australia, Perth, Western Australia, Australia, 6009

Michael McEldrew

E-mail: mpm5354@gmail.com

Department of Chemical Engineering, Massachusetts Institute of Technology, Cambridge, MA, USA

Boris Kozinsky

E-mail: bkoz@g.harvard.edu

John A. Paulson School of Engineering and Applied Sciences, Harvard University, Cambridge, MA 02138, USA

Robert Bosch LLC, Research and Technology Center, Cambridge, MA 02142, USA

Martin Z. Bazant

E-mail: bazant@mit.edu

Department of Chemical Engineering, Massachusetts Institute of Technology, Cambridge, MA, USA

Department of Mathematics, Massachusetts Institute of Technology, Cambridge, MA, USA

Cecilia Leal

E-mail: cecilial@illinois.edu

Department of Materials Science and Engineering, University of Illinois at Urbana-Champaign, Urbana, Illinois 61801, USA

Rob Atkin: Rob.Atkin@uwa.edu.au

[1]School of Molecular Sciences, The University of Western Australia, Perth, Western Australia, Australia, 6009

Andrew Gewirth

E-mail: agewirth@illinois.edu

Department of Chemistry, University of Illinois at Urbana−Champaign, Urbana, Illinois 61801, United States

Mark W. Rutland

E-mail: mark@kth.se

KTH Royal Institute of Technology, Department of Chemistry, Stockholm SE-100 44, Sweden; School of Chemistry

University of New South Wales, Sydney 2052, Australia; Laboratoire de Tribologie et Dynamique des Systèmes,

École Centrale de Lyon, Lyon 69130, France; and Bioeconomy and Health, Materials and Surface Design, RISE

Research Institutes of Sweden, Stockholm, Sweden

Rosa Espinosa-Marzal*

E-mail: rosae@illinois.edu

Department of Materials Science and Engineering, University of Illinois at Urbana-Champaign, Urbana, Illinois 61801, USA

Department of Civil and Environmental Engineering, University of Illinois at Urbana-Champaign, Urbana, Illinois 61801, USA

Classification:

Major: Physical Sciences, Minor: Chemistry

Keywords: ionic liquids, salt-in-ionic liquids, surface forces apparatus, long-range force, aggregation

Abstract

Ionic liquids (ILs) are a promising class of electrolytes owing to a unique combination of properties, such as extremely low vapour pressures, non-flammability and being universal solvents. Doping ILs with alkali metal salts creates an electrolyte that is of interest for batteries, among others. These salt-in-ionic liquids (SiILs) are a class of super-concentrated, strongly correlated and asymmetric electrolytes. The transference number of the alkali metal cations has been found to be negative, owing to the small but highly negatively charged aggregates which form between alkali metal ions and the anions. Here, we investigate Na-based SiILs with a surface forces apparatus and by atomic force microscopy. We find evidence of confinement induced structural changes, giving rise to unprecedented long-range (non-exponentially decaying) interactions. This observation is supported by the soft structure revealed by the force curves, and supplemented by theory and simulations. The long-ranged interactions in SiILs are reminiscent of polymer-like interactions, suggesting analogous high aspect ratio aggregates at the mica interfaces, rather than a purely electrostatic origin. Remarkably, our aggregation framework and conclusions can also explain the negative transference number, often observed in these systems by the battery community.

Significance statement

Ionic solutions with high concentrations play a pivotal role in next-generation energy storage technologies. To extend the current limited understanding, we study a salt-in-ionic liquid— liquid composed solely of ions— using complementary force measurements, theory and simulations. We show that ions aggregate in soft elongated large clusters that cause a long-range interaction that is not purely electrostatic. These results provides experimental and theoretical evidence that the earlier proposed dilute electrolyte electrolyte model is insufficient. This new way of envisioning concentrated ionic solutions has also implications on conductivity, intercalation and solid electrolyte interphases, which are crucial for battery operation. Hence, our findings pave the way for a new perspective on concentrated ionic solutions, offering insights that will advance energy storage applications.

\Main text

Introduction

Ionic liquids (ILs) are a highly promising class of electrolytes for myriad applications, from energy storage to solvents for reactions and lubrication.(1-3) These electrolytes, in their pure form, only comprise of ions, which gives rise to a unique combination of properties, such as being non-flammable and electrochemically stable.(4) Despite these compelling traits, ILs are limited in their direct use in battery applications, mainly owing to the cations being too large to intercalate into graphite layers and their high viscosity which leads to only moderate conductivity. (5, 6) Doping the IL with alkali metal (Li^+ or Na^+) salts bearing the same anion as the host IL, a concept known as salt-in-ionic liquid (SiIL), has the potential to benefit from the desirable properties of ILs for battery applications, where issues with electrochemical stability and flammability have persisted, (4-6) while still maintaining the conductivity of the active metal cation. (7-9)

ILs have been shown to undergo structural changes in the presence of alkali metal salts.(10-12) Electrophoretic NMR and atomistic simulations of SiILs have revealed that the alkali metal cations at small mole fractions have negative transference numbers.(8, 9, 13) Transference numbers –i.e., the ratio of the electric current derived from the cation to the total electric current– are typically within 0 to 1, and

values deviating from 0.5 are often explained by cation/anion size asymmetries. To explain negative values, however, strong correlations between the IL anion and the metal cation are invoked.(7-9) At small mole fractions of Na/Li salts, the IL anions greatly outnumber the metal cations so that Li^+/Na^+ are completely solvated by IL anions, resulting in small, highly negatively charged ionic clusters.(7-9) These ionic clusters are vehicularly transported, giving rise to the reported negative transference numbers.(14) However, when the fraction of alkali metal salt is similar to that of the IL, the Li/Na-anion aggregates interconnect, resulting in a percolating ionic network.(7-9) This leads to preferential conduction pathways that improve the mobility of the metal cation relative to the anion, and to positive transference numbers and high ionic conductivity.

While the nanostructure and transport anomaly of SiILs have been well studied, there are still many open questions, including their electrical double layer (EDL) and how it affects energy storage. Atomistic simulations of various SiILs by Haskins et al. (15) showed that Li^+ prefers to reside in the anionic layer of the overscreening structure, suggesting the strong interactions between Li^+ and the anion prevent Li^+ from directly adsorbing on the electrode surface. Li^+ introduces disorder in the EDL, but, under some conditions, it can also promote packing between anions and cations, leading to an increase in differential capacitance. (15) McDonald et al.(16) reported Atomic Force Microscopy (AFM) images of mica in propylammonium nitrate with ~60 mM of alkali metal salts. This study suggested that the metal cations preferentially adsorb to negatively charged sites on the mica surface, despite their much lower concentration compared to the IL cations.

Questions about the nature of the EDL of ILs recently arose from the experimental observations of extremely long-ranged interactions between mica and gold surfaces.(17-19) These forces were assumed to be of electrostatic origin and their large decay length was explained by the renormalization of the charge carrier concentration.(20) Investigating long-ranged interactions in SiILs, perhaps one of the most correlated electrolytes known, might also give insight into the nature of long-ranged interactions in ILs and other superconcentrated electrolytes. In this paper, we investigate surface force interactions in a SiIL composed of 1-ethyl-3-methylimidazolium bis(trifluoromethylsulfonyl)imide (abbreviated [EMIM][TFSI]) and NaTFSI.

Results

Six electrolytes were prepared under Ar atmosphere at mole fractions (x_s) of 0.008, 0.02, 0.05, 0.15, and 0.2 of NaTFSI in the SiIL (~20.6, 52, 135, 284, 451, and 639 mmol/kg IL, respectively). Force measurements between mica surfaces were carried out using an extended Surface Forces Apparatus (SFA).(21, 22) The SiILs were maintained dry *in-situ* by purging the SFA cell with a gentle stream of dry N_2, while the temperature was maintained constant at 25±0.01ºC; see Materials and Methods for further details.

As inferred from wide-angle-x ray scattering (WAXS) measurements, Na^+ alters the nanostructure of the IL; see Figure S1 in the Supplementary Information (SI). Addition of NaTFSI leads to an increase of the correlation length of the charge alternation peak from 7.02 to 7.88 Å and of the adjacency peak from 4.59 to 4.39 Å, as well as a broadening of the first peak, which points toward the decrease in order in the SiILs. This is consistent with findings for Li^+ in other imidazolium ILs,(12) but the structural changes are more significant with Na^+, presumably due to its larger size. The form factor obtained from small-angle X-ray scattering (SAXS) indicates the presence of domains of nanometer length scale, whose shape changes upon addition of salt (Figure S2).

In the first set of SFA experiments, the mica surfaces were equilibrated for 12 hours in the electrolyte to achieve mechanical and thermal equilibrium while keeping the surfaces separated by 3-5 μm. Surface force measurements were carried out at a constant velocity of 0.3 nm/s, until a maximum force of ~150 mN/m was applied, after which the surfaces were separated to D~1 μm (force-distance curve FC1) and immediately approached at the same velocity to measure the following force-distance curve (FC2). Figure 1a displays the first surface force measurement upon approach and retraction, i.e. "$FC1_{ap}$" and "$FC1_{ret}$", respectively. The subsequent force-distance curve is labeled as "$FC2_{ap}$" and "$FC2_{ret}$" for the approach and retraction, respectively. At least 2 (at most 7) experiments with different mica pairs were performed for each mole fraction and at least five force-distance curves (FC1-FC5) were measured with each pair of mica surfaces. All surface forces are repulsive. With the exception of the first approach, they are of much larger range, by at least a factor of 2, than previously reported surface forces in ILs,(17, 23, 24) with profiles that deviate from a purely exponentially decaying force. For reference, surface force measurements of the neat IL (x_s = 0) are shown in Figure S3.

Force-distance for $x_s \leq 0.10$ NaTFSI

Figure 1a-c shows FC1 and FC2 for SiILs with x_s =0.02, 0.05, and 0.10 NaTFSI at 25ºC; similar force-distance curves were obtained for x_s =0.008 NaTFSI, as shown in Figure S4a. FC1 first increases *quasi*-exponentially with decreasing surface separation (D), with a decay length of the exponential fit, d_1~ 10-12 nm, which is of the same order of magnitude than those reported for neat ILs and other highly concentrated electrolytes.(18, 19, 25) In contrast to neat ILs, when the force achieves a value F_c/R~0.84, 1.14±0.24, 2.22±0.48, and 4.03±3.44 mN/m for mole fractions x_s=0.008, 0.02, 0.05, and 0.1 NaTFSI, respectively, the surfaces undergo a *forced separation* against the driving direction over a distance of several nanometers; observed as an outward kink from separations D_c~15.3, 7.6±2.8, 7.5±4.2 and 8.9±2.4 nm, respectively. Afterwards, D starts to decrease again with a continued increase in repulsive force. This *first approach* behavior was observed in 1 of 2, 2 of 3, 3 of 4 and 6 of 7 measurements with x_s =0.008, 0.02, 0.05 and 0.1 NaTFSI, respectively.

Upon retraction of the surfaces, the force profile $FC1_{ret}$ is substantially different from $FC1_{ap}$, leading to a prominent clockwise hysteresis. $FC1_{ret}$ is only exponentially decaying (*i.e.* it is linear in semi-log plot) over intermediate length scales. A decay length d_2 ~11-19 nm was determined in the range where an exponential function can be fit, *i.e.* between the rapid decay of the force at large separations (~60-100 nm) and the steep increase close to the hard wall for $FC1_{ap}$ and $FC2_{ap}$-$FC5_{ap}$, respectively. The subsequent force-distance curves (from FC2 to FC5) are long-range, and qualitatively similar to $FC1_{ret}$; see Figure 1a;d and S5. There are only small differences between approach and retraction force curves FC2-FC5, indicating the *quasi*-reversible behavior of the SiIL after the first approach. Note that these characteristics were also observed in measurements that did not show the forced separation in $FC1_{ap}$, but in this case, the decay length of $FC1_{ap}$ was greater (*e.g.* for x_s=0.02, d_1~13.5 nm and d_2~11.34±2.6 nm, Figure S6).

A possible reason for the distinct $FC1_{ap}$ is a very slow approach to equilibrium after the SiIL is injected between the two mica surfaces which has not been achieved prior to measurement. To test this hypothesis, we measured WAXS after 2 h and 24 h of equilibration of the SiILs in their quartz capillaries (Figure S2). These indicated a subtle change in the bulk nanostructure of the liquid over time, which could have also influenced the force measurements. We performed additional SFA experiments on SiILs with x_s=0.05 NaTFSI after an equilibration time of 24 h (instead of 12 h); see Figure 1d. This indeed led to a larger surface separation for the onset of $FC1_{ap}$, closer to FC2-FC5. The forced separation in FC1 was still observed, however, at approximately the same force, but it appeared less pronounced, since it initiated at larger separation but finished at approximately the same value as after 12 h of equilibration.

Overall, these results suggest that a longer equilibration time leads to larger decay lengths of $FC1_{ap}$, but it does not remove the forced separation feature. We thus hypothesize that the variation of the surface forces must be, at least partially, associated with both the slow and subtle change of the SiIL bulk structure and the confinement of the electrolyte.

The origin of the forced separation observed in $FC1_{ap}$ was investigated in a third set of SFA experiments with x_s=0.05 NaTFSI. Here, the surfaces were approached first to various D-values larger than the distance at which the forced separation occurred in Figure 1b; see representative results in Figure S8. The data indicates that the forced separation only happens when the SiIL has been confined between the mica surfaces to a specific threshold distance, D_c. Overall, we conclude that the forced separation occurs at mole fractions between 0.02 and 0.2, after both short (12 h) and long (24 h) equilibration, and at 25ºC and 40ºC (as described later), when the SiIL is confined to a distance smaller than D_c~10 nm, all of which supports the idea of a confinement-induced phenomenon.

Force-distance curves for SiILs with $x_s \geq 0.15$

Solid precipitation was observed in SiILs with x_s=0.20 NaTFSI and the crystallization of a Na-salt was confirmed by WAXS (Figure S1a). The SiIL was filtered to prepare a saturated solution at 25 ºC, labelled as "*sat*" in the following. Precipitation was not observed at x_s=0.15 NaTFSI, and hence, the saturation mole fraction of NaTFSI at 25ºC must lie between x_s=0.15 and 0.20. Heating the SiIL with x_s=0.20 NaTFSI to 40ºC dissolved the precipitated salt, indicating that this SiIL was undersaturated at this temperature.

The main characteristics of the force-distance curves remain qualitatively unmodified at high mole fractions, $x_s \geq 0.15$ (Figure 1e): $FC1_{ap}$ increases initially quasi-exponentially with decreasing separation, with the forced separation starting at D_c~15.55 nm, and again there is a significant clockwise hysteresis between approach and retraction, with $FC1_{ret}$ being much longer range than the approach. FC2-FC5 do not perfectly decay as exponentials and exhibit only a small hysteresis. In contrast to lower concentrations, the hard wall of FC1 is located at greater separations h~16 nm at room temperature (RT) and shifts to larger values in subsequent force-distance curves; *e.g.* h~27 nm for FC2. At 40ºC (Figure 1f), the hard wall of FC1 is at h~2 nm and it remains constant in subsequent force-distance curves. The results for the saturated solution and x_s=0.20 NaTFSI at 40ºC are qualitatively similar (Figure S4b-c), implying that this behaviour is characteristic of the proximity to the saturation barrier. (In 2 of the 7 experiments carried out with SiILs with x_s=0.10, a similar shift of the hard wall was observed.) AFM images of the mica surfaces were taken at the conclusion of these SFA experiments; see Figure S8. When the shift of the hard wall had occurred, AFM images revealed the presence of nanosized aggregates with a varying number and size; in this example, they reached a maximum height of ~3 nm.

Long-range structure and oscillatory forces

Indications of a "soft" nanostructure were evident in the SFA force-distance curves, as multiple "bumps" were seen at separation distances between ~8 and 65 nm, with the majority beyond ~20 nm (**Figure 2a-b** and S9). Note that the steps are not well defined in the force-distance curves, and hence, a precise determination of their size is not possible. But a rough estimation leads to an average step size of Δ~12. 9 $\pm$4.8 Å, 15.6 $\pm$6.3 Å, 20.8 $\pm$5.7 Å, 16.3 $\pm$4.6 Å, 17.3 $\pm$8.1 Å, 15.2 $\pm$4.2 for x_s=0.008, 0.02, 0.05, 0.10, 0.15 and 0.20 NaTFSI, respectively; the step size distribution is shown in **Figure 2b**. These steps suggest that nanosized clusters in the SiILs are forced to re-arrange in layers as the mica surfaces approach each other and that these layers are progressively squeezed out as the separation distance decreases. The fact that the steps in the force-distance curves are "blurry" may be due to a cluster size

distribution and/or clusters with branches or anisotropic shapes. The force measurements were performed in a "dynamic" fashion, i.e. upon continuous approach of the surfaces at 0.3 nm/s, which might also hinder the precise detection of layer positions in viscous fluids with long characteristic times.(26) This is because the flow of the layers out of the confined film takes a finite time, and this squeeze-out is superposed to the continuous approach of the surfaces. The viscosity of the SiILs was determined with a parallel plate rheometer (Table S1, *e.g.* 59.5 mPa.s for x_s=0.10 NaTFSI). While the viscosity *could* be larger in nanoconfined films, clear steps have been previously measured in more viscous ILs confined to smaller separations.(27, 28) Based on that, we believe that the origin for the "blurry" layers relies on their size distribution, and/or anisotropic shapes.

Force-distance curves showed a *quasi*-oscillatory profile at separations beyond the onset of the repulsive force (Figure S10). This force was very small, close to the precision of the instrument, but decoupled from any temperature variation in the SFA; note that the temperature is recorded in our SFA concurrently with the surface separation, and hence, one can compare temperature and force at any point of time. Hence, we consider that this long-range *quasi* oscillatory force is not an artefact or the result of an instability. Force measurements between negatively charged surfaces in an aqueous suspension of negatively charged nanoparticles or polyelectrolytes (NPs) show that the multivalent NPs are repelled and excluded from the vicinity of the surface. If the concentration of the charged particles is high enough, their presence leads to an oscillatory structural force with the periodicity depending not on the size but on the NP volume %.(29) The *quasi* oscillatory forces could thus originate from the presence of nanosized aggregates.

Interfacial structure of SiILs

To provide further insight into the interfacial structure, force measurements were also performed with a sharp AFM tip on mica in SiILs with x_s=0, 0.05 and 0.10 NaTFSI; see Figure 3. Heat maps were constructed from multiple superposed force-distance curves. The force profiles exhibit discrete steps, which indicate that layers of ions arrange near the mica surface. Note that the position of the surface is unknown, and hence, it is possible that the ion layers that are most strongly bound to mica are not ruptured by the tip. Histograms of the surface separation were constructed to determine the layer thickness (Δ); see plots above the force-distance curves. For the neat IL (0 mol%), four layers with sizes of Δ_1~5, Δ_2~7.4, Δ_3~7.5 and Δ_4~7.1 Å were detected (Figure 3a), consistent with earlier studies.(30) Considering the negative charge of the mica surface, this nanostructure can be associated with a cation-rich ($[EMIM]^+$) layer closest to the surface (~5 Å). IL anion and cation are of similar size (Figure S11), and hence, it is not possible to distinguish between either ion pairs, anion- or cation enrichment beyond the first layer.

Fewer layers were resolved with increasing mole fraction of NaTFSI (Figure 3b). With x_s=0.05, only three layers were clearly resolved, with a different size distribution. Closest to the mica surface, Δ_1~2.1 Å, the layer is likely rich in Na^+, which displaces (most of) the $[EMIM]^+$. The size of the second layer Δ_2~6.7 Å is likely associated with the presence of anions. The size of the third layer (Δ_2~9 Å) is greater than that expected for [EMIM][TFSI], which suggests that larger complexes of cations and anions approach the surface. Further away, the tip appears to detect a similar structure as for the neat IL.

Increasing x_s to 0.10 significantly modified the interfacial structure. Only two layers were clearly resolved (Figure 3c), even when the applied force was increased to 12 nN. The thicknesses of the near-surface layers are Δ_1=8.5 Å, and Δ_2=9.4 Å, respectively, *i.e.* larger than Δ_1 and Δ_2 at lower mole fractions. This suggests that small clusters or aggregates of ions arrange in layers close to the surface,

consistent with the idea of an increase in characteristic cluster size near the mica surface with salt concentration.

Theory and simulations

To understand the structure of SiILs, we performed molecular dynamics (MD) simulations at four mole fractions of NaTFSI, $x_s \approx 0.05, 0.1, 0.15, 0.2$ at a temperature of 25ºC, with the details of the calculations in the Methods, and further results at 85ºC in the SI. First, we computed the number of coordinating $TFSI^-$ around each Na^+. $EMIM^+$ aggregation effects were not analyzed, as they are known to be significantly weaker than NaTFSI associations.(7, 31) **Figure 4a** shows that the most common number of coordinating $TFSI^-$ for $x_s = 0.05$ is 4, but 3 and 5 are also found; Figure S12 show similar results for other mole fractions, while Figure S13 displays the O-coordination distributions. Note that the relative humidity in experiments was maintained below 3% RH, and generally closer to 1% RH, which must be considered as very dry condition. Nonetheless, water uptake is expected to increase with x_s and thus, it could influence the experimental results. This has been neglected here but future work will address the incorporation of trace water into simulations.

The cluster distribution, *i.e.* the relative concentration of each aggregate with l cations and m anions, was also computed. At x_s=0.05, the dominant species is free anions, as to be expected from the large excess of $TFSI^-$ relative to Na^+. The next most prevalent species involves 4 $TFSI^-$ with 1 Na^+, but there are also few aggregates with 2 Na^+; see their respective structures and length scales in **Figure 4b** and the cluster distribution in **Figure 4c**. As x_s increases, the prevalence of these aggregates dramatically increases, as does the concentration of even larger aggregates; see Figure S14. For examples, at x_s=0.2 (**Figure 4d**), free anions and 4 $TFSI^-$ coordinated to Na^+ are still the most prevalent species, but now there are aggregates containing up to 10-20 Na^+ and 30-50 $TFSI^-$, which exhibit branched polymer-like morphologies. Owing to the larger number of $TFSI^-$ compared to Na^+ ($l > m$) constituting each aggregate, all aggregates are negatively charged, as inferred from the cluster distribution above the diagonal in **Figure 4c-d**. There is no indication of an ionic network percolating throughout the whole simulation box (referred to as a gel), which indicates the gel point in simulations is slightly higher than x_s=0.2. The length scale of the clusters is 8.8, 10.4, 12.4 and 15.6 Å for $x_s = 0.05, 0.1, 0.15$, and 0.2, respectively, and hence, it increases with mole fraction. These values agree reasonably well with the layer size close to the mica surface measured by AFM, which suggests these clusters adsorb on the mica surface despite their negative charge, presumably due to the overscreening of the negative surface charge by counterions.

The cluster bond density (CBD), i.e. the number of bonds per ion in an aggregate,(32) quantifies how ordered the aggregates are; **Figure 4e** and Figure S15. If the clusters exhibit a perfect Cayley tree structure, CBD is given by $(l+m-1)/(l+m)$ (solid line), which tends to 1 for large aggregates. We find that most aggregates reside at CBD=1.1-1.5, which is above the Cayley tree limit of 1, indicating the onset of loops. These loops indicate the aggregates are more ordered than Cayley tree clusters, which could give rise to the onset of crystalline phases; this is only observed for x_s=0.2 NaTFSI by WAXS (Figure S1). Overall, our simulations demonstrate the presence of large, charged aggregates, the size and charge of which increase with x_s. Many of these aggregates have highly branched polymer-like morphologies, but there are also more ordered aggregates that resemble nanoparticles. We believe these aggregates are the origin of the observed behavior in AFM and SFA experiments, as discussed later.

Next, we apply a newly developed theory to describe the EDL of SiILs; see ref. (33) and Methods. **Figure 4f** shows the changes in the volume fraction of Na^+ ($\overline{\phi}_+$), $TFSI^-$ ($\overline{\phi}_-$) and $EMIM^+$ ($\overline{\phi}_\oplus$) in the EDL of a SiIL with x_s=0.05. At negative voltages, the $EMIM^+$ first populates and saturates the EDL, as it does not interact strongly with $TFSI^-$, but Na^+ exchanges with $EMIM^+$ at moderate negative voltages, as it

can reach higher charge densities, which requires breaking the associations with $TFSI^-$. Within the EDL, that would mean Na^+ sits right next to the interface, and $EMIM^+$ further from it. A similar conclusion was inferred from AFM experiments at x_s=0.05 (**Figure 2b**). At positive voltages, $TFSI^-$ accumulates at the surface and $EMIM^+$ depletes monotonically in the EDL, but there is a tiny increase in Na^+ at intermediate voltages. **Figure 4g** displays the volume fractions of free $TFSI^-$ ($\overline{\phi}_{10}$), free Na^+ ($\overline{\phi}_{01}$) and aggregates ($\overline{\phi}_{11\geq}$) and shows a large peak in aggregates within the EDL at moderate positive voltages. This is associated with a plateau of free $TFSI^-$, as the additional $TFSI^-$ is being used to build the aggregates with Na^+ that are dragged into the EDL. Thus, there are electric field induced associations at positive voltages, and these aggregates effectively screen the electrode charge.

The theory also predicts the screening length of the SiIL (λ_s); see calculation in Methods and ref. (33). With increasing x_s, λ_s decreases from 0.12 nm to 0.105 nm. This is because a higher x_s dramatically promotes aggregate formation and their multivalency actually increases the ionic strength. This has also been confirmed by the MD simulations (see Figure S16). Therefore, the change of the theoretical screening length with mole fraction is qualitatively different from the experimental force decay length (d_1 and d_2, **Figure 3c**), and confirms that a simple screening theory cannot be used to explain the long-range forces of SiILs. In summary, theory and MD simulations support the contention that the origin of these forces is not an electrostatic repulsion, but occurs from other effects arising from the aggregation of ions into large, highly charged branched polymer-like structures and more ordered nanoparticles.(32) We elaborate further the connection to SFA experiments in the Discussion Section.

Discussion

The force-distance curves for this SiIL are significantly different to those measured for neat [EMIM][TFSI], which display (i) an exponentially decaying force with a decay length of ~ 6.5 nm, (ii) a short range (structural) force reflecting the layered arrangement of the IL ions with a step width of ~ 7.5 Å, and (iii) good agreement with subsequent force-distance curves, *i.e.* a reversible behavior. The novel observations of the SiIL are thus the forced separation, "soft" structure of the electrolyte at large separation, slow equilibration times (*i.e.*, long relaxation times), and the difference between first and subsequent approaches, which are almost certainly all linked phenomena. An explanation thus needs to self-consistently address all observations, as well as being consistent with other properties of the electrolytes, such as conductivity.(14)

The influence of a "soft" structure on the long-ranged forces has been reported for a water-in-salt-electrolyte (WiSE) with LiTFSI.(34) This WiSE exbibits a cluster-like nanostructure in the bulk, as inferred from small angle neutron scattering and MD simulations.(35, 36) In SFA measurements,(34) the onset of the repulsive force can be as large as ~80 nm. As these clusters become confined between the mica surfaces, they are forced to re-arrange in layers, which appears as "subtle" steps superposed to the surface forces. SFA measurements revealed an increasing cluster size with concentration, ranging from 1 to 3.3 nm in the range ~8-18 m LiTFSI in water. At 8 m, the less prominent long-range structure in force curves is a clear indication of the vanishing nanostructure of the bulk electrolyte. Closer to the surface, the structural size is smaller and less dependent on concentration (0.80−0.99 nm), revealing the significant influence of the surface on the nanostructure. These results suggest an origin of the long-range surface forces based on the aggregation behavior of the WiSE, and by extension for this SiIL, although the less clear steps in force-distance curves of the latter could reflect a greater disorder in the electrolyte.

We have provided evidence that the interfacial behavior of this SiIL strongly deviates from that expected for an electrolyte according to Debye-Hückel theory. Even if the classical EDL theory of dilute

electrolytes were to be invoked, the presence of multivalent coions (*i.e.* negatively charged aggregates) would likely eliminate the observation of an exponentially decaying electrostatic force.(29) Despite this, an exponential function was fitted to the force-distance curves to enable a comparison to reported decay lengths of neat ILs, and other highly concentrated electrolytes.(25) As x_s increases, the values of d_1 (diamonds) and d_2 (circles) increase to ~14.1 and 19 nm, respectively (**Figure 2c)**, while there is no distinction between d_1 and d_2 for the neat IL (~6.5$\pm$ 0.5 nm). It is difficult to reconcile these observations with an exponential electrostatic model. All this has motivated us to propose an alternative approach within an aggregation framework.

Conceptually, our theory is based on the analogy between highly concentrated electrolytes and polymers,(32) with highly branched polymer-like aggregates being predicted by theory and simulations. One could then draw an analogy between the long-range repulsion and that arising from the compression of a charged polymer film between mica surfaces in a reservoir of solvent. A simple model for an osmotic polyelectrolyte brush(37) was thus tested to describe FC2-FC5; see SI. As shown in **Figure S17**, the fits are satisfactory at $x_s \leq 0.10$. One of the fitting parameters is the area per charge, ranging between 0.63 to 0.98 nm^2 (**Table S2**), which is reasonable in comparison to what is expected for SiIL aggregates. The surface forces in SiILs with higher x_s-values can be still fit by the same model, but one needs to account for the shift of the hard wall (not shown). Notably, the size of the aggregates found in the bulk SiIL – according to theory and simulations– is significantly smaller than the range of the force. Thus, instead of the small aggregates attached to the mica surface, as shown in AFM experiments, the confining geometry of the SFA appears to induce the formation of larger aggregates. Next, we shall describe how the discrepancy between AFM and SFA measurements is linked to the *forced separation* in FC1, hysteresis, and slow dynamics.

Complex surface forces have been reported for nanoparticle suspensions in water,(38) with significant hysteresis between approach and separation in FC1 and a prominent difference between FC1 and subsequent force-distance curves, which are of much shorter range, in contrast to our results. Regions of near-constant force –inward kinks– are observed in the force curves and associated with a change of volume at constant pressure, and therefore, with a first-order transition; specifically, the disorder-to-order transition of the nanoparticles of different shapes (spheres, rods and wires) when they are forced to arrange between the mica surfaces. This disorder-order transition leads to an inward step, while here an outward kink (forced separation) is observed, and hence, these must be different phenomena.

The difference between FC1 and the following force-distance curves is intriguing, and has not been reported for ILs, as far as the authors are aware. At the mole fractions of our experiments, the theory does not predict the onset of a fully percolating ionic network (gelation) in the bulk SiIL, but instead, the presence of clusters in a liquidous SiIL. FC1 initially resembles the long-range force in an IL, but, at a certain characteristic force (F_c/R) and separation (D_c,) a transition occurs to a state with a larger characteristic length. This larger characteristic length presumably arises due to the presence of larger aggregates between the mica surfaces, which are, likely, confinement-induced. Note that the disorder-to-order (sponge-like to lamellar) transition in ILs was proposed to be templated by a "flat" interfacial cation layer. (39) Perhaps, the first approach (FC1) modifies (flattens) the interfacial cation layer and this induces a transition of the confined SiIL to a state of smaller density, and thus, greater volume or characteristic length. It is also possible that an enhancement in the local Na^+ concentration results from the preferential adsorption of Na^+ to the mica surface (as further outlined in the SI) and/or the non-stoichiometric expulsion of ions upon approach of the surfaces. The latter assumes that $EMIM^+$ is more weakly bound to $TFSI^-$ than Na^+, which implies that EMIM-TFSI ion pairs could be expelled more easily than large Na-TFSI aggregates, resulting in a local increase in Na^+ concentration. Na^+ enrichment

between the mica surfaces could cause the onset of a percolating ionic network between the mica surfaces and lead to a local, and robust transition to a state with a larger characteristic length scale. This transition into interconnected (branched polymer- or nanogel-like) aggregates could propagate laterally throughout the confined region (radius of the order of a micrometer, **Figure 2d**). Such a confinement-induced transition should not be confused with the related phenomena of, for example capillary condensation(40) or capillary induced polymer separation,(41) which cause an interface to be formed between a (different) confined phase and the bulk, and therefore an attractive force. Rather one should see this as an acceleration towards equilibrium, with local inhomogeneity. There is no interface, *per se*.

The proposed transition would lead to a difference in chemical potential with respect to the bulk, where smaller clusters exist. Invoking an imbalance of the chemical potential between the larger aggregates in equilibrium with the supersaturated solution in the confined region ($\mu_{l,conf}$) and the bulk SiIL ($\mu_{l,0}$) leads to a mechanical work $\Delta p \cdot V$ that pushes the mica surface away, causing the forced separation. The measured force for this transition (F/R~2 to 5 mN/m) implies a pressure between 1 and 40 MPa, which leads to c_{conf}/c_{bulk}~1.1-10, assuming V_m=141 cm^3/mol for NaTFSI; see details in the SI. That is, the concentration of clusters in the confined region becomes ~1.1-10 times larger than in the bulk for the range x_s from 0.008 to 0.1, which triggers further aggregation and even gelation. Subsequent separation of the surfaces draws these larger aggregates into the gap between the surfaces (**Figure 2d**). The surface force in following compressions can be understood to result from an osmotic pressure driving the swelling of the nanogel-like aggregates and an electrostatic component, where the ionic units no longer correspond to the individual ions but to strings of coordinated ions. Although the small hysteresis between approach and retraction force curves FC2-FC5 implies that hydrodynamics cannot justify the long-range of the surface forces, it might also have a small effect. The absence of a pull-off force in retraction force-curves indicates that bridging between the aggregates adsorbed on both surfaces is not possible, as expected for crosslinked polyelectrolyte films and nanogels.

Interestingly, a longer equilibration before approach (12 h vs. 24 h, **Figure 1b;d**) typically maintained the forced separation but it was less significant. Furthermore, in the experiments where the forced transition was not measured (in the range of low concentration), the force still became longer range, presumably suggesting that the percolation/interconnection between clusters happened, but less "abruptly", *i.e.* more continuously during approach and retraction, leading to the same equilibrium state.

The subtle differences between the force-distance curves (FC2, and subsequent) point at the slow dynamics in the SiILs after percolation being induced under confinement, possibly transitioning slowly toward equilibrium, and consistent with the long relaxation times inferred from simulations for another SiIL.(8, 9) WAXS measurements (Figure S1) also showed a slow change in the bulk structure of the SiILs, which might contribute to the variation of the surface forces. There is also reported evidence for an ultra-slow transition in common imidazolium ILs, namely, 1-ethyl-3-methyl imidazolium ethylsulphate and 1-hexyl-3-methyl imidazolium [TFSI].(42) WAXS experiments revealed the gradual ordering of the ions in domains of ~10 nm size while adopting a 1D lamellar structure; over a similar period of time, SFA measurements showed the evolution of the surface force. In that study, a relation between the domain ordering in the IL and the variation of the surface force was suggested. Here, we propose a similar relationship for a stronger correlated electrolyte.

The shift of the hard wall observed at high mole fractions is presumably also associated with surface- or confinement-induced nucleation of large aggregates. Note that a confinement-induced solidification was also reported for 1-hexyl-3-methyl imidazolium ethylsulphate between mica surfaces, and it also appeared as a continuous shift of the hard wall.(43) Although crystallization is observed in unconfined SiIL at

x_s=0.2 and 25ºC, we do not have any evidence for the crystallinity of the aggregates formed between the mica surfaces. Indeed, nucleation can follow a non-classical pathway,(44) where prenucleation clusters (often, chain-like ionic clusters) precede the formation of amorphous intermediates (via aggregation), which may then transition into a crystal, or instead, kinetically remain in an amorphous state. Even according to classical nucleation, the lifetime of amorphous metastable precursors becomes dramatically longer under confinement, while the nucleation rate of crystalline phases is significantly reduced.(45) Note that we refer to the confinement-induced formation of (charged) branched polymer- and nanogel-like clusters based on i) MD simulations and theory, and ii) its compressibility in experiments, but such a structure is not very different from the concept of prenucleation clusters and amorphous precursors based on non-classical and classical nucleation, respectively. It is thus possible that at the highest x_s-values investigated here, the formation of larger and/or a higher number of aggregates is further promoted in the confined region, which is reflected as a significant shift of the hard wall.

In conclusion, the described experiments and theory of SiILs close to a negatively charged surface appear to be unified by the presence of clusters and their confinement-induced aggregation, which explains, among others, the action of long-range forces despite the small screening length. This work thus provides experimental and theoretical evidence that, for complex associating systems such as SiILs, a dilute electrolyte EDL model(20) is insufficient. It cannot be ruled out that such association can occur in other IL systems, leading to similar long-range interactions, but that for weaker association of IL ions these non-exponential forces are not measureable. Furthermore, the aggregation occurring close to charged surfaces likely has implications for the formation of solid electrolyte interphases and for intercalation, which are crucial for battery operation.

Materials and Methods

Sodium bis(trifluoromethylsulfonyl)imide (NaTFSI, 99.5%, Solvionic) was dried at 120°C under vacuum for 12 hours. [EMIM][TFSI] (97%, Sigma-Aldrich) was dried at 50°C under vacuum in a Fisher Scientific Isotemp vacuum oven for 48 hours. Both were stored in an Ar-filled glovebox, containing <1 ppm of O_2 and <1 ppm of H_2O. Six electrolytes were prepared under Ar atmosphere with mole fractions (x_s) 0.008, 0.02, 0.05, 0.10, 0.15 and 0.20 of NaTFSI. They were mixed in a THINKY AR-100 conditioning mixer for three sessions of three minutes. The solutions were investigated within 1 week after preparation. All samples were filtered with a 200 nm syringe filter before the measurements.

The force measurements with an extended SFA(21, 22) were conducted following well-established procedures.(24) A volume of ~500 μL SiIL was injected into the space between two mica surfaces in the fluid cell of the SFA. During force measurements, the cell was purged with dry N_2 while the relative humidity in the cuvette was constantly monitored with a sensor (Sensirion, Switzerland) located roughly 1 cm above the surfaces. The dry nitrogen maintained the relative humidity below 3% RH during the SFA experiments, which is labeled as “dry” condition. The temperature of the system was maintained at either 25$\pm$0.02 ºC or 40$\pm$0.05 ºC with a home-built temperature-control device.(22) The system was equilibrated for either 12 or 24 hours to minimize mechanical and thermal drifts, after which one of the surfaces was driven to approach the other at a constant velocity of 0.3 nm/s.

Force measurements were also conducted using a JPK (Santa Barbara, CA) atomic force microscope (AFM) and CSC-37 silicon tips (MikroMasch, CA), with nominal spring constant ~0.6 N/m as determined by the thermal noise method(46) and a nominal tip radius of ~10 nm. Prior to the measurement, the cantilevers were cleaned by UV ozone for 20 minutes. AFM force measurements were obtained on freshly cleaved mica surfaces. The tip velocity was set at 20 nm/s. A total of 64 force curves were collected on an area of 500 nm by 500 nm at each concentration. At least two force maps were

carried out per sample. Tapping mode AFM images were captured using a Cypher VRS AFM (Asylum Research, Oxford Instruments) and a JPK AFM. Images with a scan size of 500 nm × 500 nm were taken at a scan rate of 8 Hz with soft cantilevers (0.09 ± 0.03 N/m, BL-AC40TS, Olympus). At least three different areas were imaged on each sample. The AFM cell was sealed and purged with dry N_2.

To perform the molecular dynamics (MD) simulations of NaTFSI in [EMIM][TFSI], we followed the method outlined by Molinari et al. in (8, 9). The OPLS-AA force fields(47) for these ions were utilized, but the charge was rescaled to take into account effects from polarizability.(8, 9) For x_s ≈0.05, 0.1, 0.15, 0.2, there are 7, 15, 23, 32 Na^+, 150, 155, 159, 164 $TFSI^-$ and 143, 140, 136, 132 $EMIM^+$, respectively. MD simulations were conducted in LAMMPS(48) at temperatures of 25ºC or 85ºC and at atmospheric pressure and used the equilibration procedure in refs. (8, 9) to ensure the structures found their lowest energy state, before 500 uncorrelated frames were collected for further analysis. A total of 5 simulations at each mole fraction and temperature were run to ensure good statistics. The collected 2500 frames were used to calculate properties of the aggregates, such as the cluster distribution and cluster bond density.

It is known that $EMIM^+$ only weakly interacts with $TFSI^-$ in comparison to Na^+.(7, 31) To define the associations between Na^+ and $TFSI^-$, a real space cutoff of 3.65 Å was used, as this corresponds to the first minimum in the pair correlation function between Na and TFSI. We used this information to build an adjacency matrix between the Na-TFSI clusters for the calculation of coordination numbers, cluster distribution and cluster bond density. To estimate the average length scale of clusters, the weight average degree of aggregation was modified as shown in the SI. We also calculated the relative ionic strength using a similar expression; see SI.

The MD simulations also allowed to extract the parameters of the theory developed in ref. (7) for SiILs. We found that Na^+ has a maximum of f_+=5 associations, and $TFSI^-$ a maximum of f_-=3 associations; note that the results are not very sensitive to small changes in these values and a f_+ = 4 could be more appropriate. The volume of a lattice site was taken to be that of Na^+, while $EMIM^+$ and $TFSI^-$ are approximately 7 times this size. The association probability between the ions was obtained by dividing the coordination number of $TFSI^-$ around Na^+ by f_+ and used in the mass action law to find the association constant at each mole fraction to be 20.2, 22.9, 25.7, 30.1, respectively. From fitting the concentration dependence of the association constant, we decoupled the free energy of an association between Na-TFSI and [EMIM][TFSI] regular solution interaction. This led to values of the free energy of association and regular solution interaction to be -8.4 and 7.1, respectively. These values indicate stronger interactions than in previously investigated SiILs,(7) especially the regular solution term, but as we only have data over a limited concentration range to perform the fit, we are not confident in these values. Only the overall association constant is well known at each concentration, which is found to be smaller than for Li-based SiILs.

Our theory is inspired on the free energy functional by Flory, Stockmayer and Tanaka, which was modified first for the bulk(7, 31, 49) and later to handle electrified interfaces.(50) Here, we draw on the previous work on salt-in-ionic liquids (SiILs) from McEldrew *et al.(7)* and extend it to the electrical double layer (EDL) using the formalism of Goodwin *et al.(50)*

The system is composed of IL cations and anions, denoted by, respectively, $\oplus$ and $-$, and alkali metal cations, denoted by $+$. The volume fraction of each species, ϕ_j, is known in the bulk. The size of the alkali metal cation is υ_+, with the volumes of the other species being given by $\upsilon_+\xi_i$, where $\xi_i = \upsilon_i/\upsilon_+$. The unitless concentration of each species is given by $c_j = \phi_j/\xi_j$.

The alkali metal cations are assumed to form a maximum of f_+ associations and the anions a maximum of f_- associations, referred to as the functionality of each species. If both the functionalities are larger than 1, a polydisperse cluster distribution of clusters of rank *lm* can form, where *l* is the number of alkali metal cations and *m* the number of anions. A key assumption is that only Cayley-tree-like clusters can also form.(49) A percolating ionic network can form for both functionalities larger than 2.(49) This is referred to as the gel here. In the gel regime, we employ Flory's convention to determine the volume fractions of each species in the gel/sol, where $\phi_{+/-} = \phi_{+/-}^{sol} + \phi_{+/-}^{gel}$.

The free energy functional is taken to be:

$$\begin{aligned} \upsilon_+\mathcal{F} = \int_V d\mathbf{r}\ & -\frac{\upsilon_+\epsilon_0\epsilon_r}{2}(\nabla\Phi)^2 + \upsilon_+\rho_e\Phi + k_BTc_\oplus \ln\phi_\oplus + \sum_{lm}(k_BTc_{lm}\ln\phi_{lm} + c_{lm}\Delta_{lm}) \\ & + \int_V d\mathbf{r}\chi\phi_\oplus \sum_{lm}(f_-m - m - l + 1)c_{lm} + \Delta_+^{gel}c_+^{gel} + \Delta_-^{gel}c_-^{gel} \\ & + \int_V d\mathbf{r}k_BT\Lambda\left(1 - \xi_\oplus c_\oplus - \sum_{lm}(l + \xi_- m)c_{lm}\right) \end{aligned} \tag{1}$$

Where $\Phi(\mathbf{r})$, $\rho_e(\mathbf{r}) = \frac{e}{\upsilon_+}(c_\oplus + c_+ - c_-)$, and, $\phi(\mathbf{r})/c(\mathbf{r})$ are, respectively, the electrostatic potential, charge density, and volume fractions/dimensionless concentrations. Here, the free energy of forming clusters of rank *lm* is given by Δ_{lm}, χ is the regular solution interaction between the IL cations and the open association sites, Δ_j^{gel} is the free energy of species associating to the gel, and Λ is the Lagrange multiplier to enforce the incompressibility.

The free energy of forming a cluster of rank *lm* has two contributions

$$\Delta_{lm} = \Delta_{lm}^{comb} + \Delta_{lm}^{bind} \tag{2}$$

the combinatorial entropy and the binding free energy. The combinatorial entropy for Cayley trees is given by

$$\Delta_{lm}^{comb} = k_BT\ \ln\{f_+^l\ f_-^m\ W_{lm}\} \tag{3}$$

where

$$W_{lm} = \frac{(f_+l - l)!\,(f_-m - m)!}{l!\,m!\,(f_+l - l - m + 1)!\,(f_-m - m - l + 1)!}. \tag{4}$$

The binding free energy for Cayley trees is given by

$$\Delta_{lm}^{bind} = (l + m - 1)\Delta f_\pm \tag{5}$$

From the free energy we can calculate all properties of our system, both in the bulk and the EDL. From establishing the chemical equilibrium between free species and clusters of rank *lm*, we can arrive at the cluster distribution:

$$c_{lm} = \frac{W_{lm}}{\lambda}(\lambda f_+ \phi_{10})^l \, (\lambda f_- \phi_{01}/\xi_-)^m \tag{6}$$

Here λ is the ionic association constant, given by

$$\lambda = exp\left\{\beta\left(-\Delta f_\pm + \chi\phi_\oplus\right)\right\} = \lambda_0 \, exp\left\{\beta\chi\phi_\oplus\right\} \tag{7}$$

Crucially, the cluster distribution depends on the volume fraction of free species, i.e., those not bound to any other species, and should be calculated by theory. This problem is overcome by introducing ion association probabilities, p_{ij}, which is the probability that an association site of species *i* is bound to species *j*, where *i* and *j* are either the alkali cation (+) or the IL anion (−).(7) Therefore, the volume fraction of free alkali cations can be written as $\phi_{10} = \phi_+(1 - p_{+-})^{f_+}$and free anions as $\phi_{01} = \phi_-(1 - p_{-+})^{f_-}$.(7)

The association probabilities can be determined through the conservation of associations and a mass action law between open and occupied association sites.(7, 49) The conservation of associations is given by

$$p_{+-}\psi_+ = p_{-+}\psi_- \tag{8}$$

where $\psi_+ = f_+\phi_+$ and $\psi_- = f_-\phi_-/\xi_-$ are the number of alkali cation and anions association sites per lattice site, respectively.(7, 49) The mass action law between open and occupied association sites is given by:

$$\lambda\zeta = \frac{p_{+-}p_{-+}}{(1 - p_{+-})\,(1 - p_{-+})} \tag{9}$$

where $\zeta = \psi_- p_{-+} = \psi_+ p_{+-}$ is the dimensionless concentration of associations (per lattice site).(7, 49)

Following the work of Goodwin *et al.*,(50) we connect the bulk and EDL cluster distributions to the Poisson equation through closure relations. Equating the chemical potential of the free ions in bulk and in the EDL allows us to write down three additional equations:

$$\bar{\phi}_{10} = \phi_{10} \exp(-e\beta\Phi + \Lambda) \tag{10}$$

$$\bar{\phi}_{01} = \phi_{01} \, exp(e\beta\Phi - \beta\chi f_-(\bar{\phi}_\oplus - \phi_\oplus) + \xi_-\Lambda) \tag{11}$$

$$\bar{\phi}_\oplus = \phi_\oplus \exp\left(-e\beta\Phi + \beta\chi f_-\xi_\oplus\{c_-(1 - p_{\mp}) - \bar{c}_-(1 - \bar{p}_{\mp})\} + \xi_\oplus\Lambda\right) \tag{12}$$

Note a bar is used to denote EDL quantities. These closure relations can be solved as a function of Φ to determine the EDL properties of the system from solving the Poisson equation. Although the parameters

extracted from MD simulations can be used in the theory, they led to strong gelation at positive voltages and sharp features in the results. Due to the lack of confidence in the exact values of the free energy of association and regular solution interaction, we chose to employ the parameters previously found in ref. (7), as these have a lower tendency to push the system to the gel regime.

Acknowledgements

This material is based upon work supported by the National Science Foundation under grants DMR-1904681, and CBET 1916609 to REM. MR acknowledges support from the Swedish Research Council, VR (Project No. 2017-04080), and the Swedish Foundation for Strategic Research (Project No. EM16-0013, "REFIT"). R.M.E.M. also thanks Prof. Manfred Heuberger (EMPA) for discussions about confinement-induced transitions and the extended SFA and Roland Kjellander for insightful discussions about electrolyte theory. Work at MIT by M.M. and M.Z.B. was supported from an Amar G. Bose Research Grant. D.M.M. also acknowledges support from the National Science Foundation Graduate Research Fellowship under Grant No. 2141064. Work at MIT by D.M.M. and M.Z.B. was supported as part of the Center for Enhanced Nanofluidic Transport (CENT), an Energy Frontier Research Center funded by the U.S. Department of Energy (DOE), Office of Science, Basic Energy Sciences (BES), under award # DE-SC0019112. The work at Harvard was supported by the Department of Navy award N00014-20-1-2418 issued by the Office of Naval Research.

References

1. T. Welton, Room-Temperature Ionic Liquids. Solvents for Synthesis and Catalysis. *Chemical Reviews* **99**, 2071-2084 (1999).
2. M. Armand, F. Endres, D. R. MacFarlane, H. Ohno, B. Scrosati, Ionic-liquid materials for the electrochemical challenges of the future. *Nat Mater* **8**, 621-629 (2009).
3. C. Ye, W. Liu, Y. Chen, L. Yu, Room-temperature ionic liquids: a novel versatile lubricant. *Chem Commun (Camb)* 10.1039/B106935G, 2244-2245 (2001).
4. G. G. Eshetu *et al.*, Electrolytes and Interphases in Sodium-Based Rechargeable Batteries: Recent Advances and Perspectives. *Advanced Energy Materials* **10**, 2000093 (2020).
5. K. Xu, Electrolytes and Interphases in Li-Ion Batteries and Beyond. *Chemical Reviews* **114**, 11503-11618 (2014).
6. M. Watanabe *et al.*, Application of Ionic Liquids to Energy Storage and Conversion Materials and Devices. *Chemical Reviews* **117**, 7190-7239 (2017).
7. M. McEldrew *et al.*, Salt-in-Ionic-Liquid Electrolytes: Ion Network Formation and Negative Effective Charges of Alkali Metal Cations. *The Journal of Physical Chemistry B* **125**, 13752-13766 (2021).
8. N. Molinari, J. P. Mailoa, B. Kozinsky, General Trend of a Negative Li Effective Charge in Ionic Liquid Electrolytes. *J Phys Chem Lett* **10**, 2313-2319 (2019).
9. N. Molinari, J. P. Mailoa, N. Craig, J. Christensen, B. Kozinsky, Transport anomalies emerging from strong correlation in ionic liquid electrolytes. *Journal of Power Sources* **428**, 27-36 (2019).

10. T. Murphy, S. K. Callear, G. G. Warr, R. Atkin, Dissolved chloride markedly changes the nanostructure of the protic ionic liquids propylammonium and ethanolammonium nitrate. *Phys Chem Chem Phys* **18**, 17169-17182 (2016).
11. R. Hayes, S. A. Bernard, S. Imberti, G. G. Warr, R. Atkin, Solvation of Inorganic Nitrate Salts in Protic Ionic Liquids. *The Journal of Physical Chemistry C* **118**, 21215-21225 (2014).
12. L. Aguilera, J. Völkner, A. Labrador, A. Matic, The effect of lithium salt doping on the nanostructure of ionic liquids. *Phys Chem Chem Phys* **17**, 27082-27087 (2015).
13. M. Gouverneur, F. Schmidt, M. Schönhoff, Negative effective Li transference numbers in Li salt/ionic liquid mixtures: does Li drift in the "Wrong" direction? *Phys Chem Chem Phys* **20**, 7470-7478 (2018).
14. D. Monti, E. Jónsson, M. R. Palacín, P. Johansson, Ionic liquid based electrolytes for sodium-ion batteries: Na+ solvation and ionic conductivity. *Journal of Power Sources* **245**, 630-636 (2014).
15. J. B. Haskins, J. J. Wu, J. W. Lawson, Computational and Experimental Study of Li-Doped Ionic Liquids at Electrified Interfaces. *The Journal of Physical Chemistry C* **120**, 11993-12011 (2016).
16. S. McDonald, A. Elbourne, G. G. Warr, R. Atkin, Metal ion adsorption at the ionic liquid–mica interface. *Nanoscale* **8**, 906-914 (2015).
17. M. A. Gebbie *et al.*, Ionic liquids behave as dilute electrolyte solutions. *Proceedings of the National Academy of Sciences of the United States of America* **110**, 9674-9679 (2013).
18. M. A. Gebbie *et al.*, Long range electrostatic forces in ionic liquids. *Chem Commun (Camb)* **53**, 1214-1224 (2017).
19. R. M. Espinosa-Marzal, Z. A. H. Goodwin, X. Zhang, Q. Zheng, "Colloidal Interactions in Ionic Liquids—The Electrical Double Layer Inferred from Ion Layering and Aggregation" in One Hundred Years of Colloid Symposia: Looking Back and Looking Forward. (American Chemical Society, 2023), vol. 1457, chap. 7, pp. 123-148.
20. A. A. Lee, C. S. Perez-Martinez, A. M. Smith, S. Perkin, Underscreening in concentrated electrolytes. *Faraday Discuss* **199**, 239-259 (2017).
21. M. Heuberger, The extended surface forces apparatus. Part I. Fast spectral correlation interferometry. *Review of Scientific Instruments* **72**, 1700-1707 (2001).
22. M. Heuberger, J. Vanicek, M. Zäch, The extended surface forces apparatus. II. Precision temperature control. *Review of Scientific Instruments* **72**, 3556-3560 (2001).
23. R. M. Espinosa-Marzal, A. Arcifa, A. Rossi, N. D. Spencer, Ionic Liquids Confined in Hydrophilic Nanocontacts: Structure and Lubricity in the Presence of Water. *The Journal of Physical Chemistry C* **118**, 6491-6503 (2014).
24. R. M. Espinosa-Marzal, A. Arcifa, A. Rossi, N. D. Spencer, Microslips to "Avalanches" in Confined, Molecular Layers of Ionic Liquids. *J Phys Chem Lett* **5**, 179-184 (2014).
25. A. M. Smith, A. A. Lee, S. Perkin, The Electrostatic Screening Length in Concentrated Electrolytes Increases with Concentration. *J Phys Chem Lett* **7**, 2157-2163 (2016).
26. L. Bureau, Rate Effects on Layering of a Confined Linear Alkane. *Phys Rev Lett* **99**, 225503 (2007).
27. M. Han, R. M. Espinosa-Marzal, Electroviscous Retardation of the Squeeze Out of Nanoconfined Ionic Liquids. *The Journal of Physical Chemistry C* **122**, 21344-21355 (2018).
28. M. Han, S. A. Rogers, R. M. Espinosa-Marzal, Rheological Characteristics of Ionic Liquids under Nanoconfinement. *Langmuir* **38**, 2961-2971 (2022).
29. L. R. J. Scarratt, K. Kubiak, P. Maroni, G. Trefalt, M. Borkovec, Structural and Double Layer Forces between Silica Surfaces in Suspensions of Negatively Charged Nanoparticles. *Langmuir* **36**, 14443-14452 (2020).
30. R. Hayes, S. Z. El Abedin, R. Atkin, Pronounced Structure in Confined Aprotic Room-Temperature Ionic Liquids. *The Journal of Physical Chemistry B* **113**, 7049-7052 (2009).
31. M. McEldrew, Z. A. H. Goodwin, H. Zhao, M. Z. Bazant, A. A. Kornyshev, Correlated Ion Transport and the Gel Phase in Room Temperature Ionic Liquids. *The Journal of Physical Chemistry B* **125**, 2677-2689 (2021).

32. Z. A. H. Goodwin, M. McEldrew, B. Kozinsky, M. Z. Bazant, Theory of Cation Solvation and Ionic Association in Nonaqueous Solvent Mixtures. *PRX Energy* **2**, 013007 (2023).
33. D. M. Markiewitz *et al.*, Electric Field Induced Associations in the Double Layer of Salt-in-Ionic-Liquid Electrolytes. *arXiv preprint arXiv:2402.04039* 10.48550/arXiv.2402.04039 (2024).
34. M. Han, R. Zhang, A. A. Gewirth, R. M. Espinosa-Marzal, Nanoheterogeneity of LiTFSI Solutions Transitions Close to a Surface and with Concentration. *Nano Letters* **21**, 2304-2309 (2021).
35. O. Borodin *et al.*, Liquid Structure with Nano-Heterogeneity Promotes Cationic Transport in Concentrated Electrolytes. *ACS Nano* **11**, 10462-10471 (2017).
36. L. Suo *et al.*, "Water-in-salt" electrolyte enables high-voltage aqueous lithium-ion chemistries. *Science* **350**, 938-943 (2015).
37. P. Pincus, Colloid stabilization with grafted polyelectrolytes. *Macromolecules* **24**, 2912-2919 (1991).
38. M. Akbulut *et al.*, Forces between Surfaces across Nanoparticle Solutions: Role of Size, Shape, and Concentration. *Langmuir* **23**, 3961-3969 (2007).
39. R. Hayes, G. G. Warr, R. Atkin, At the interface: solvation and designing ionic liquids. *Phys Chem Chem Phys* **12**, 1709-1723 (2010).
40. H. K. Christenson, Non-Dlvo Forces Between Surfaces -Solvation, Hydration and Capillary Effects. *Journal of Dispersion Science and Technology* **9**, 171-206 (1988).
41. H. Wennerström, K. Thuresson, P. Linse, E. Freyssingeas, Long Range Attractive Surface Forces Due to Capillary-Induced Polymer Incompatibility. *Langmuir* **14**, 5664-5666 (1998).
42. M. Han *et al.*, Insight into the Electrical Double Layer of Ionic Liquids Revealed through Its Temporal Evolution. *Advanced Materials Interfaces* **7**, 2001313 (2020).
43. L. A. Jurado *et al.*, Irreversible structural change of a dry ionic liquid under nanoconfinement. *Phys Chem Chem Phys* **17**, 13613-13624 (2015).
44. D. Gebauer, H. Cölfen, Prenucleation clusters and non-classical nucleation. *Nano Today* **6**, 564-584 (2011).
45. M. L. Whittaker, P. M. Dove, D. Joester, Nucleation on surfaces and in confinement. *MRS Bulletin* **41**, 388-392 (2016).
46. J. E. Sader, J. W. M. Chon, P. Mulvaney, Calibration of rectangular atomic force microscope cantilevers. *Review of Scientific Instruments* **70**, 3967-3969 (1999).
47. W. L. Jorgensen, D. S. Maxwell, J. Tirado-Rives, Development and Testing of the OPLS All-Atom Force Field on Conformational Energetics and Properties of Organic Liquids. *Journal of the American Chemical Society* **118**, 11225-11236 (1996).
48. S. Plimpton, Fast Parallel Algorithms for Short-Range Molecular Dynamics. *Journal of Computational Physics* **117**, 1-19 (1995).
49. M. McEldrew, Z. A. H. Goodwin, S. Bi, M. Z. Bazant, A. A. Kornyshev, Theory of ion aggregation and gelation in super-concentrated electrolytes. *J Chem Phys* **152**, 234506 (2020).
50. Z. A. H. Goodwin, M. McEldrew, J. Pedro de Souza, M. Z. Bazant, A. A. Kornyshev, Gelation, clustering, and crowding in the electrical double layer of ionic liquids. *J Chem Phys* **157**, 094106 (2022).

Figures and Tables

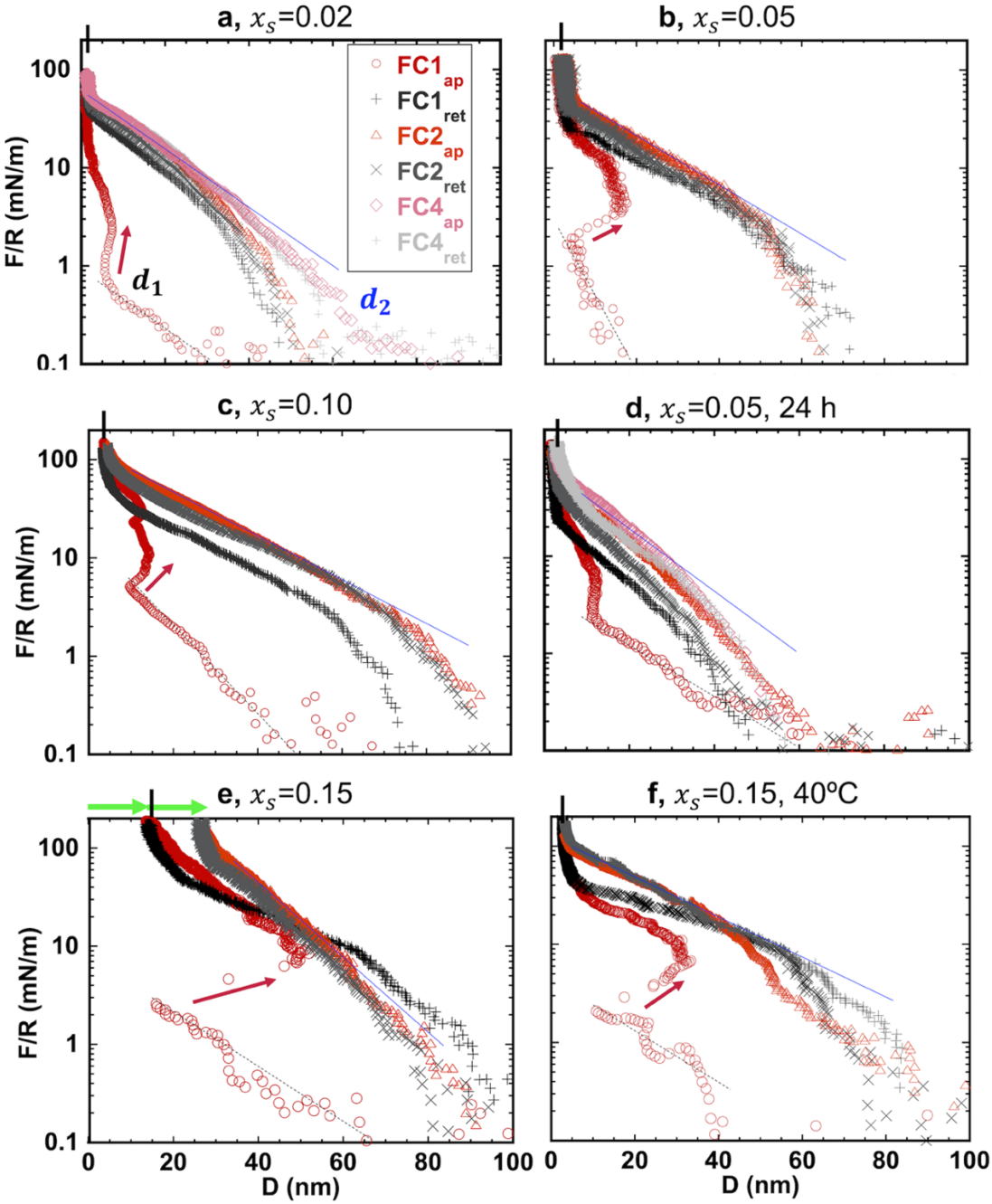

Figure 1. Representative surface forces between mica surfaces for various mole fractions of NaTFSI. Force-distance curves for mole fractions (x_s) **a,** 0.02, **b,** 0.05, **c,** 0.10, **e,** 0.15, after 12 hours equilibration, 25ºC; **d,** x_s=0.05 after 24 hours equilibration at 25ºC**, f,** x_s=0.15 at 40ºC after 12 h equilibration. The plots show $FC1_{ap}$ (red circles), $FC1_{ret}$ (black cross), $FC2_{ap}$ (red triangles), and $FC2_{ret}$ (grey x-marks). a and d) also show force-distance curves FC4. The black and blue lines show exponential fits with decay lengths d_1 and d_2, respectively. Green arrow in e shows the shift of the hard wall during force measurements. Each force-distance curve displays the force normalized by the radius of the surface, F/R, *vs.* the surface separation.

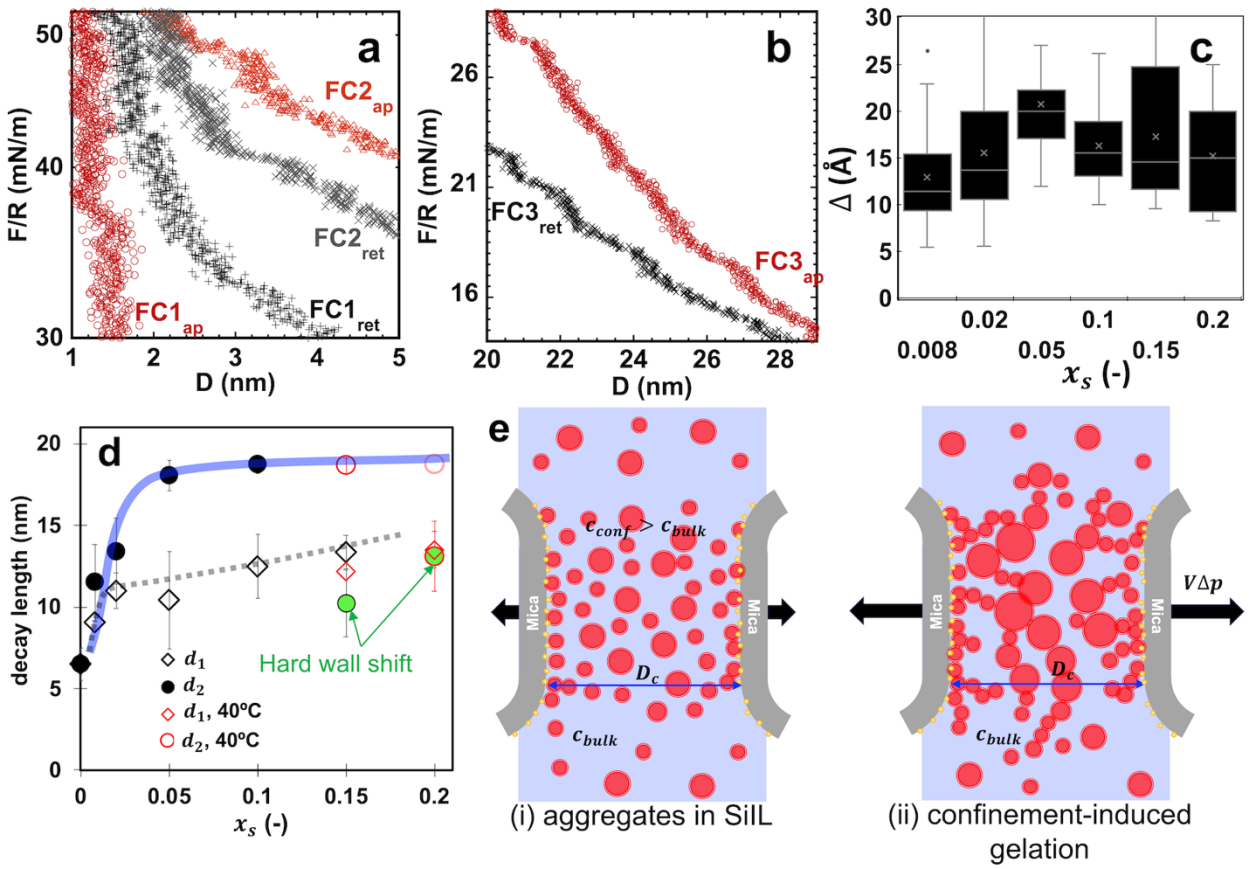

Figure 2. Relation between decay length and long-range structure of SiILs. **a-b,** Examples of steps in SFA force-distance curves; see also Figure S9. The inset in b shows the distribution of step size. **c,** Decay length of $FC1_{ap}$ (d_1) and $FC2_{ap}$-$FC5_{ap}$ (d_2) as a function of mole fraction of NaTFSI, at 25 and 40ºC. The decay lengths influenced by the shift of the hard wall are shown with green markers. For x_s=0.2 at 40ºC, d_2 is 18.9 nm (semitransparent red marker) before the shift of the hard wall, but d_2 decreases to 13.1±2.6 nm, when the hard wall shifts. The values for the saturated solution at 25ºC (for d_1~3.3 nm and d_2~14.1 0.6 nm, with significant shift of the hard wall) are not shown, since the actual mole fraction of NaTFSI after filtering the precipitate is unknown. **d,** Conceptual picture of the confinement-induced gelation of this SiIL causing the forced separation. The yellow circles represent Na^+ partially screening the negative charge of the mica surface; IL ions and aggregates are shown in blue and red, respectively. We assume aggregate concentration is enhanced when the surfaces are approached so that $c_{conf} > c_{bulk}$. At a critical surface separation D_c, gelation is triggered, and the imbalance in the chemical potential inside and outside the pore justifies the mechanical work exerted by the branched polymer- and nanogel-like aggregates against the mica surface, $V_{gel}\Delta p$. In subsequent force measurements, the osmotic pressure gradient justifies the enhanced repulsion.

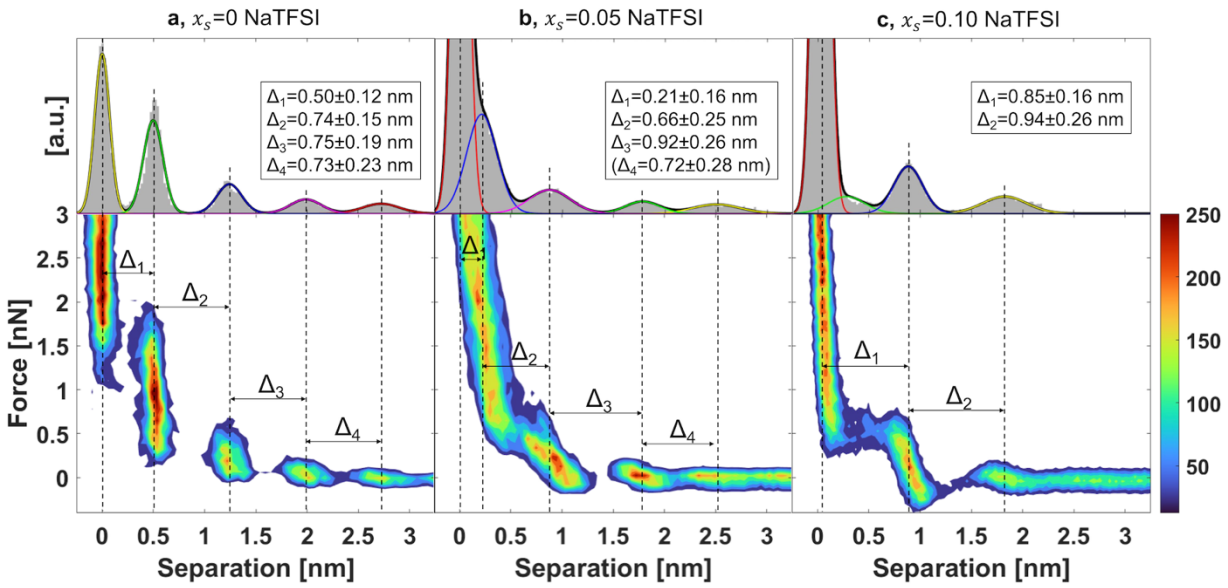

Figure 3. AFM force-distance curves in dry SiILs with x_s **a,** 0, **b,** 0.05 and **c,** 0.10 NaTFSI in equilibrium with dry nitrogen. The mica surface was equilibrated for 2 hours with the SiIL before measurements started. Each plot shows a heat map of superposed force-distance curves (34 in a, 46 in b and 63 in c). Results were reproducible in other spots of the mica surface. Dimensions of IL cation 4 Å x 7.5 Å x 1.7 Å and of IL anion 3 Å x 7.6 Å x 2.5 Å (see molecular structure of the IL in Figure S11).

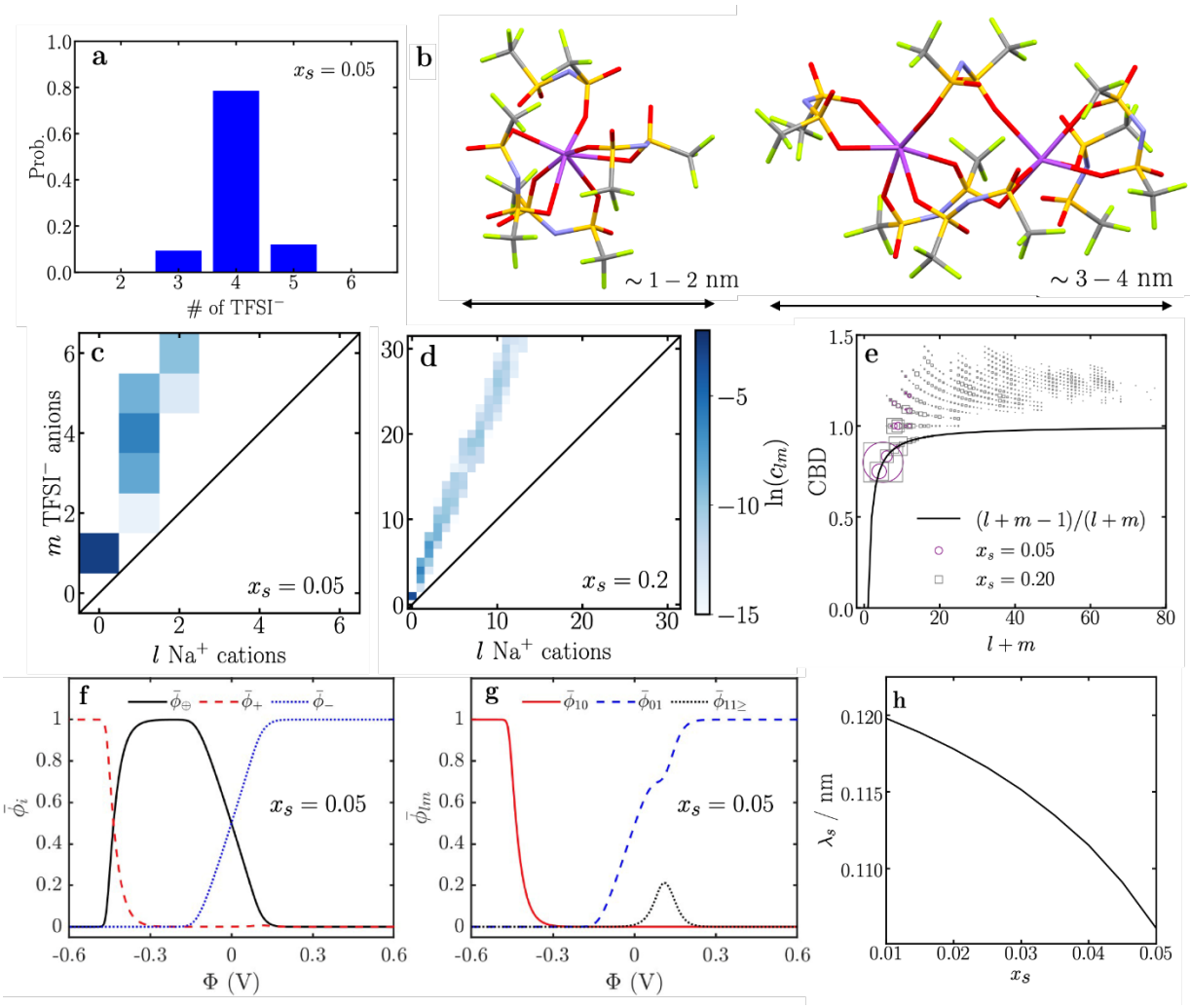

Figure 4. **Theory and simulation of ionic aggregation in the bulk and at charged interfaces. a,** Probability distribution of number of $TFSI^-$ bound to Na^+ for x_s= 0.05. **b,** Structures and length scales of example clusters for a single Na^+ and two Na^+. **c-d**, Distribution concentration of TFSI-Na aggregates (c_{lm}, in dimensionless units) composed of m $TFSI^-$ and l Na^+, for x_s = 0.05 and 0.2, respectively. **e**, Cluster bond density (CBD); the solid line denotes the Cayley tree limit given by $(l+m-1)/(l+m)$. **f**, Volume fraction of ions and **g**, volume fraction of free Na^+, free $TFSI^-$ and aggregates in the EDL, both as a function of applied potential Φ. **h**, Screening length λ_s from the theory in function of x_s.